

A multiwavelength analysis of an electron-dominated gamma-ray event associated with a disk solar flare

G rard Trottet¹, Nicole Vilmer¹, Claude Barat², Arnold Benz³, Andreas Magun⁴, Alexandr Kuznetsov⁵, Rachid Sunyaev⁵, and Oleg Terekhov⁵

¹ DASOP, CNRS-URA 2080, Observatoire de Paris, Section de Meudon, F-92195 Meudon, France

² Centre d'Etude Spatiale des Rayonnements, BP 4346, F-31029 Toulouse, France

³ Institute of Astronomy, ETH-Zentrum, CH-8092 Z rlich, Switzerland

⁴ University of Bern, IAP, Sidlerstrasse 5, CH-3012 Bern, Switzerland

⁵ Space Science Institute, Profsoyuznaya 84/32, 117810 Moscow, Russia

Received 19 November 1997 / Accepted 6 March 1998

Abstract. This paper reports the first comparison of hard X-ray (HXR), gamma-ray (GR), centimetric-millimetric and metric-decimetric spectral and imaging radio observations obtained during an electron-dominated gamma-ray burst. This impulsive event, which occurred on 1990 June 11 at ~ 0943 UT, was associated with a H_{α} 2B flare, located close to the disk center. The time evolution of the HXR emission consists of successive peaks of ~ 10 s duration. Several of these peaks show GR emission up to a few MeV and one of them up to ~ 56 MeV. For each of these peaks, the photon spectrum significantly hardens above a break energy varying in the 0.4–0.7 MeV range. No significant GR line (GRL) emission is detected. The main results of our analysis are: (i) even if no significant GRL emission is detected, the upper limit of the energy content in > 1 MeV/nucleons is comparable with the energy content in > 20 keV electrons (a few 10^{29} ergs), as it is found for GRL flares; (ii) during the whole event, the centimetric-millimetric emission is radiated by $\gtrsim 0.4$ –0.7 MeV electrons which have been accelerated since the very beginning of the flare; (iii) the different HXR/GR peaks are associated with step-wise changes of the magnetic structures to which metric-decimetric radio producing electrons have access. This latter characteristic of the 1990 June 11 burst is globally similar to the behaviour reported in the literature for GRL events, but the energy in accelerated particles is about one order of magnitude lower. Finally, the electron-dominated emitting peak with emission up to ~ 56 MeV is interpreted as a signature of an upward moving population of relativistic electrons which is strongly beamed along the magnetic field and which does not contribute significantly to the centimetric-millimetric and $\lesssim 0.2$ MeV HXR emissions. The metric-decimetric radio observations indicate that this happens when electrons have suddenly access to large-scale magnetic structures.

Key words: Sun: activity – Sun: flares – Sun: particle emission – Sun: radio radiation

1. Introduction

Extensive hard X-ray (HXR) and gamma-ray (GR) observations performed over the past two decades have established that acceleration of both bremsstrahlung (sometimes up to > 10 MeV) producing electrons and GR line (GRL) producing ions is a common feature of solar flares (e.g. Chupp 1996 and references therein). Even if a single acceleration process cannot by itself accelerate electrons and ions in a wide energy band (Miller et al. 1997), there is strong evidence that the two particle species are in most events energized simultaneously. Indeed: (i) there is a close similarity between the time evolution of the HXR/GR electron bremsstrahlung continuum and that of the prompt GRL emission from 1–100 MeV/nucleons (e.g. Forrest & Chupp 1983; Chupp 1990; Talon et al. 1993a; Trottet et al. 1993a); (ii) when the statistics are sufficient, GRL emission has been measured at the very beginning of some flares, before the fast rise of the HXR emission (Chupp et al. 1993; Trottet et al. 1994; Debrunner et al. 1997). A number of studies has shown moreover that there is a rough correlation between the HXR electron bremsstrahlung fluence and the GRL one, down to the sensitivity limit for GRL detection by the Gamma-Ray Spectrometer on the Solar Maximum Mission (e.g. Forrest 1983; Vestrand 1988; Vestrand 1991; Cliver et al. 1994). This supports the idea that energetic electrons and ions may be accelerated in all flares. Furthermore, it has been recently estimated that the total ion energy content above 1 MeV/nucleon is comparable to the total electron energy content above 20 keV (Ramaty et al. 1995). There is however a strong variability of the bremsstrahlung component compared to the nuclear line component (i.e. of the relative efficiency of electron acceleration with respect to ion acceleration), from one flare to another (see Fig. 3 in Miller et al. 1997) and even during a given flare (Chupp et al. 1993; Marschh user et al. 1983). In this context, the observations of short duration (a few seconds to a few tens of seconds) bremsstrahlung (> 10 MeV) transient bursts occurring any time during a flare (Rieger 1994) are challenging. These bursts, referred to as electron-dominated events (Rieger & Marschh user 1990), are characterised by weak or

no detectable GRL emission and by hard $\gtrsim 0.8$ -1 MeV electron bremsstrahlung spectra which extend up to a few tens of MeV (Marschhäuser et al 1983). The apparent lack of GRL emission in these bursts does not necessarily contradict the possibility that electrons and ions are produced in all flares. Indeed, Cliver et al. (1994) noticed that, given the relative values of the >50 keV photon flux and of the upper limit of the GRL fluence in these events, they do not constitute a special class of bursts and seem to follow the general correlation observed between the two fluences. Electron-dominated transient bursts thus appear as an extreme case of variability of accelerated electron and ion contents.

Multiwavelength studies of a few events, combining HXR, GR, optical and radio observations, have indicated that, during a flare, changes in the spectra of both electrons and ions are associated with the appearance of new coronal radio emitting sources and/or new H_{α} eruptive sites (Raoult et al. 1985; Wülser et al. 1990; Chupp et al. 1993; Trottet et al. 1993b; Trottet et al. 1994). This led to the idea that the small ($\sim 10^3$ - 10^4 km) and large ($\sim 10^5$ km or more) scale magnetic structures involved in particle acceleration and transport do not remain the same in the course of a flare and that the characteristics of the accelerated population are dependent on these magnetic structures. It was furthermore suggested that the relative efficiency of electron versus ion acceleration strongly depends upon the physical conditions (magnetic field, density, temperature,...) which characterize the magnetic structures involved at a peculiar time in the flare development (e.g. Trottet 1994 and references therein). At present these conclusions have been drawn from the analysis of HXR flares and of a few flares with strong GRL emission.

In this paper we have carried out the first multiwavelength analysis of an electron-dominated event associated with a H_{α} flare located close to the solar disk center. We have performed a detailed analysis of the 0.1-100 MeV HXR/GR measurements and of millimeterwave to meterwave spectral and imaging radio observations. As in the previous multiwavelength studies of GRL events, we estimated the total energy content in electrons and ions, studied the time evolution of the bremsstrahlung spectrum and its relationship with the evolution of the magnetic structures inferred from the metric-decimeteric radio data, discussed the relationship between bremsstrahlung and centimetric-millimetric emitting electrons and investigated under which conditions > 10 MeV bremsstrahlung emission can be observed from a disk flare.

2. Description of instrumentation

The HXR/GR observations were made with the PHEBUS experiment on board the French-Russian GRANAT mission. PHEBUS consists of six detectors with axes parallel to the cartesian coordinate system of GRANAT (Barat et al. 1988). Each detector is a cylindrical BGO scintillator with a diameter of 7.8 cm and a length of 12 cm surrounded by a plastic anticoincidence shield. Two of the six detectors, which have their axis essentially perpendicular to the Earth-Sun line, are suitable for solar flare observations. In this study of the 1990 June 11 flare, we have

analyzed observations obtained by one of these two detectors from 0942:48 UT till 0954:03 UT. These observations consist of 39 channel spectra in the 0.12-90 MeV energy range. Until 0943:25 UT the spectra are recorded with a variable accumulation time (time to spill mode). Afterwards the accumulation time is 1 second below 10 MeV and 4 seconds above 10 MeV.

The centimetric-millimetric observations were carried out with the Bern polarimeters at 3.1, 5.2, 8.4, 11.8, 19.6, 35 and 50 GHz. The total solar flux including circular polarization was sampled every 0.1 s during the event. Due to problems with receiver gain switching at the lowest frequency the flux at 3.1 GHz has saturated during the peak from 0943:40 till 0944:11 UT. The data were calibrated with absolute values of the quiet sun published in the Solar Indices Bulletin (NGDC, Boulder, Colorado). Observed quiet sun fluxes above 15.4 GHz are not available on a regular basis. Therefore values of 700, 2400, and 4500 sfu have been taken for 19.6, 35.0 and 50 GHz (Croom 1979). These values are typically independent of non flare solar activity (S-component) that becomes prominent below 10 GHz. The observed quiet sun data before the burst and the data from sky observations were used to calibrate the burst fluxes within an error of approximately $\pm 10\%$. In order to reduce noise, especially at higher frequencies, all flux time profiles were smoothed over a time interval of 1s (running mean) before analysis.

The metric and decimetric spectral radio observations (100 MHz-3 GHz) have been obtained by two spectrometers of ETH Zürich. The PHOENIX digital instrument is a frequency-agile receiver fully controlled by a microcomputer (Benz et al. 1991). It has recorded 20 selected channels below 1 GHz and 180 equally spaced channels between 1.0 and 3.0 GHz. The flux density and circular polarization (Stokes V parameter) were measured with a time resolution of 0.1s. The channel width above 1 GHz was 10 MHz, below it was 1 or 3 MHz selected to avoid terrestrial interferences. The second spectrometer (DAEDALUS, Tarnstrom 1973) is a swept-frequency instrument continuously recording the full 100-1000 MHz range on film. The film has been scanned yielding digital data with a resolution of about 2 MHz and 0.3 s. The low-frequency channels of PHOENIX have been used to calibrate the DAEDALUS data in frequency, time and flux density. The data of both spectrometers can be analyzed in the forms of spectra, time profiles or spectrograms.

Radio imaging observations in the metric-decimeteric range were obtained with the Nançay Radioheliograph (NRH) (The Radioheliograph group 1983, 1989). The 1990 June 11 flare was recorded with the Mark IV version of the NRH which provides one dimensional images (total intensity and circular polarization) in the east-west (EW) direction at 164 MHz and in the north-south direction (NS) at 164 MHz, 236.6 MHz, 327 MHz, 408 MHz and 435 MHz. During the 1990 June 11 event, the spatial resolution of the NS array, inversely proportional to the observing frequency, was $3.8'$ at 164 MHz. Four images per second were recorded at each frequency. The EW array operated only at 164 MHz with a spatial resolution of $1.6'$ and a time resolution of 0.02 seconds. At 164 MHz the EW and NS one dimensional images allow us to obtain the 2-d position of the centroids of the emitting sources, projected on the solar disk.

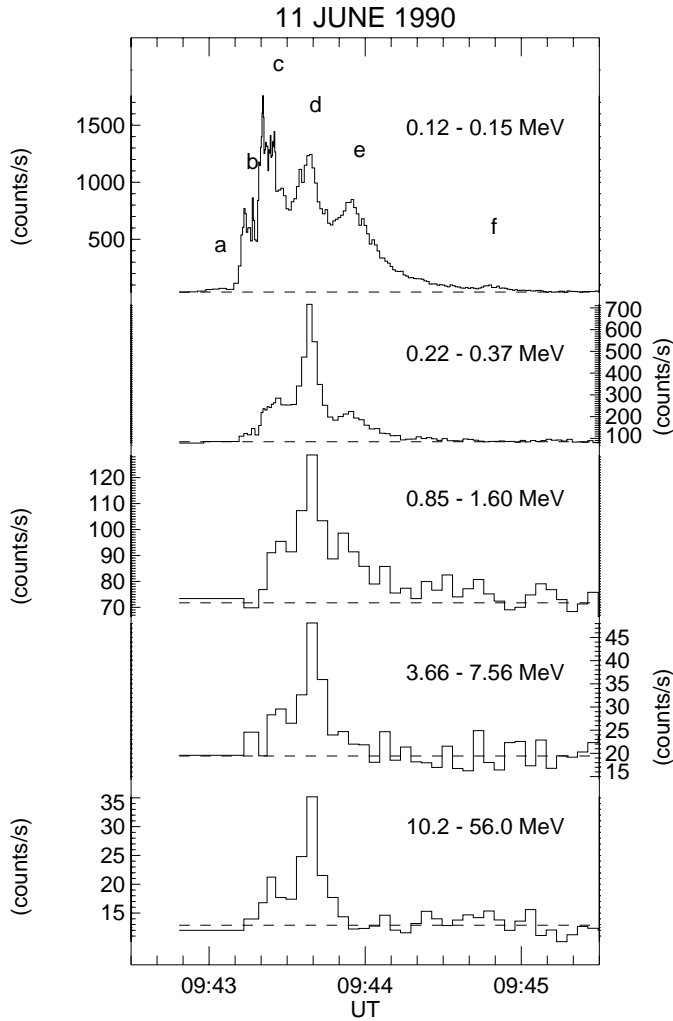


Fig. 1. The time evolution of the HXR/GR count rate recorded by PHEBUS in different energy bands. For each energy band, the dotted line indicates the background count rate.

At the other frequencies, only NS images are available and the projection on the solar disk of the actual position of a given source lies along a straight line. The accuracy of absolute position measurements is about $0.2'$ and $0.5'$ for the EW and NS arrays respectively.

3. Multi-wavelength observations of the 1990 June 11 flare

3.1. Hard X-ray and gamma-ray observations

The 1990 June 11 $H\alpha$ 2B (GOES M4.5) flare occurred in NOAA region 6089 (N10 W22) at 0934 UT. This flare was detected in the HXR/GR domain by PHEBUS from about 0942:56 UT to about 0945 UT. Former studies of the 1990 June 11 HXR/GR burst (Talon et al. 1993b; Vilmer et al. 1994a) have shown that, despite its short duration, the time structure of the ~ 100 keV count rate is complex. It exhibits both fast variations on sub-second time-scales and slower ones on time-scales ranging from a few seconds to a few tens of seconds. The present analysis only considers these latter variations.

Table 1. Onset and end times of the HXR/GR emission in different energy bands (see text)

Energy (MeV)	Onset time (UT)	End time (UT)
0.12-0.15	0942:59 \pm 3s	0944:56 \pm 1s
0.22-0.37	0943:12 \pm 4s	0944:14 \pm 2s
0.50-0.66	0943:19 \pm 4s	0943:58 \pm 4s
0.85-1.60	0943:22 \pm 3s	0943:58 \pm 4s
3.66-7.56	0943:26 \pm 4s	0943:46 \pm 4s
10.20-56.00	0943:34 \pm 4s	0943:46 \pm 4s
56.00-90.00	No flux	No flux

Table 2. Photon spectrum parameters obtained for the different HXR/GR peaks and for the whole event (see text for the definition of the parameters)

	A (at 0.1 MeV) ($\text{ph}(\text{cm}^2\text{MeVs})^{-1}$)	γ_1	γ_2	E_b (MeV)
a	≈ 18	≈ 4		
b	564 ± 100	5.0 ± 0.1		
c	1053 ± 50	4.4 ± 0.1	2.0 ± 0.1	0.36 ± 0.05
d	566 ± 30	2.9 ± 0.1	1.7 ± 0.1	0.74 ± 0.10
e	619 ± 60	4.2 ± 0.1	2.0 ± 0.1	0.38 ± 0.05
f	≈ 37	≈ 4		
S	357 ± 50	4.0 ± 0.1	2.0 ± 0.1	0.35 ± 0.05

Fig. 1 displays the time evolution of the HXR/GR count rate detected in five energy bands. The time intervals when the enhanced count-rate in different energy bands is at least 3σ above the background are reported in Table 1. The onset of the HXR/GR emission occurs progressively later, the higher the photon energy. Such energy dependent delays in the onset times of the HXR/GR emission have been also reported by Klein et al. (1987) and Chupp et al. (1993).

The 0.12-0.15 MeV count rate exhibits broad peaks marked a, b, c, d, e and f in Fig. 1. Among the four most intense ones (b, c, d, e), only peak d shows significant ($> 3\sigma$ above background) emission in the 10-56 MeV band. Peak c is only associated with a marginally significant ($< 3\sigma$ above background) emission above 10 MeV around 0943:22UT. Spectral analysis was performed for count spectra accumulated on time intervals corresponding to these six peaks. A trial photon spectrum, defined by a set of free parameters, is convolved with the detector response function to construct a test count spectrum. A χ^2 minimization algorithm is used to determine the free parameters providing a test count spectrum which reasonably fits the observed one. The fit is considered acceptable when the reduced χ^2 is ≈ 1 and when the uncertainties in all fitted parameters are smaller than the parameters themselves. For the six peaks it is found that a photon spectrum represented by a single or a double power law leads to a reasonable agreement between test and observed count spectra. Table 2 displays the values of the parameters de-

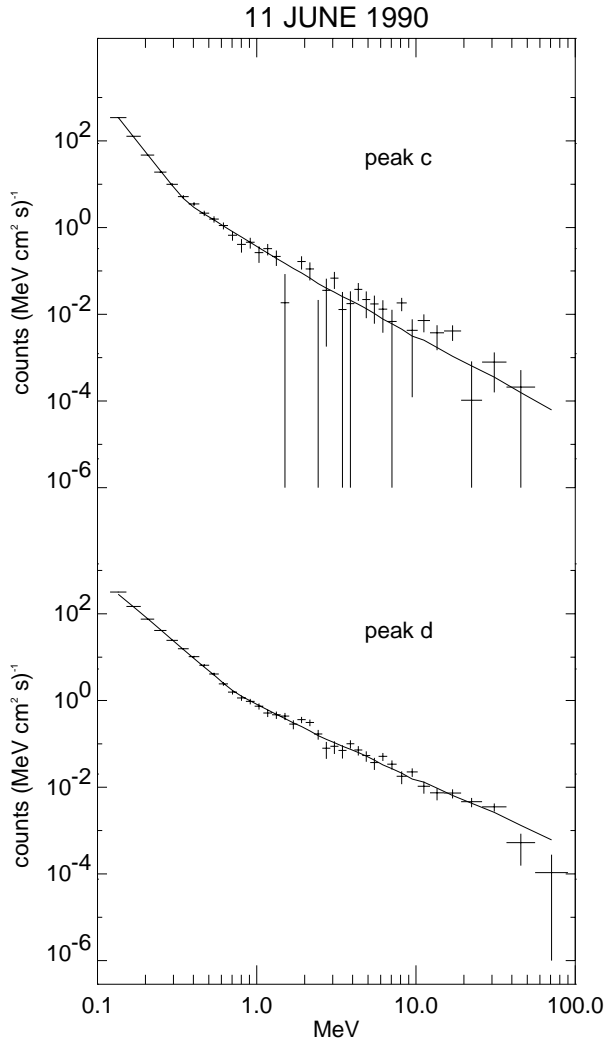


Fig. 2. Background subtracted HXR/GR count spectra observed by PHEBUS during peaks c and d (errors bars). For each spectrum, the solid curve represents the best fit model (see Table 2)

terminated for each of the six peaks and for S, the count spectrum accumulated over the whole event from 0943 to 0945 UT.

1. For peaks a, b and f, significant emission is only detected at low energies so that a single power law photon spectrum, given by $A(h\nu)^{-\gamma_1}$ was considered. The free parameters are thus A (photons $\text{cm}^{-2} \text{MeV}^{-1} \text{s}^{-1}$), the photon flux at 0.1 MeV, and γ_1 the power law index. Due to the low count rate, these parameters are poorly determined for peaks a and f, and we just take the results as an indication that $\gamma_1 \approx 4$.
2. For peaks c, d and e, where significant > 1 MeV emission is detected, it is necessary to consider a double power law to obtain a satisfactory representation of the measured count spectra. This is illustrated in Fig. 2 where the test count spectra (solid lines) have been overplotted on the observed ones (1σ error bars) for peaks c and d. The free parameters are then A and γ_1 as before, E_b the break energy and γ_2 the power law index for $h\nu > E_b$. Table 2 indicates that during peaks c and e, the photon spectrum has a similar

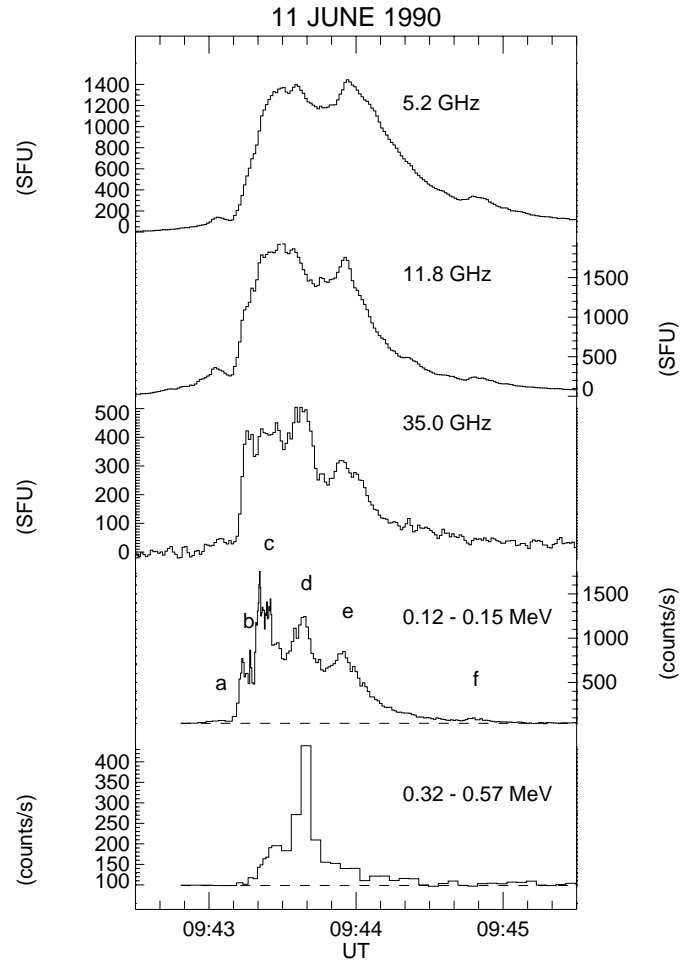


Fig. 3. Comparison of the time evolution of the centimetric-millimetric flux density observed by the Bern polarimeters at 5.2 GHz, 11.8 GHz and 35 GHz with that of the HXR/GR detected by PHEBUS in the 0.12-0.15 MeV and 0.32-0.57 MeV energy bands

shape. During peak d, E_b is shifted to a significantly higher photon energy and the whole spectrum is harder, the larger hardening occurring below E_b . Fig. 2 shows that there is no significant excess ($> 3 \sigma$) above the expected count spectra in the 1-8 MeV energy range. This indicates that prompt GRL as well as the 2.23 MeV neutron capture line are not significantly detected. The 2.23 MeV line is also lacking during the decay phase of the event. Moreover during peak d there is a significant spectral rollover above ~ 56 MeV. The present analysis confirms earlier suggestions made by Talon et al. (1993a) and by Vilmer et al. (1994b) that the spectral characteristics of the 1990 June 11 event are similar to those obtained by Rieger & Marschhäuser (1990) for electron-dominated events, i. e.: (i) GRL emission, if produced, is weak; (ii) the HXR/GR spectrum extends beyond 10 MeV and exhibits a high energy rollover around a few tens of MeV.

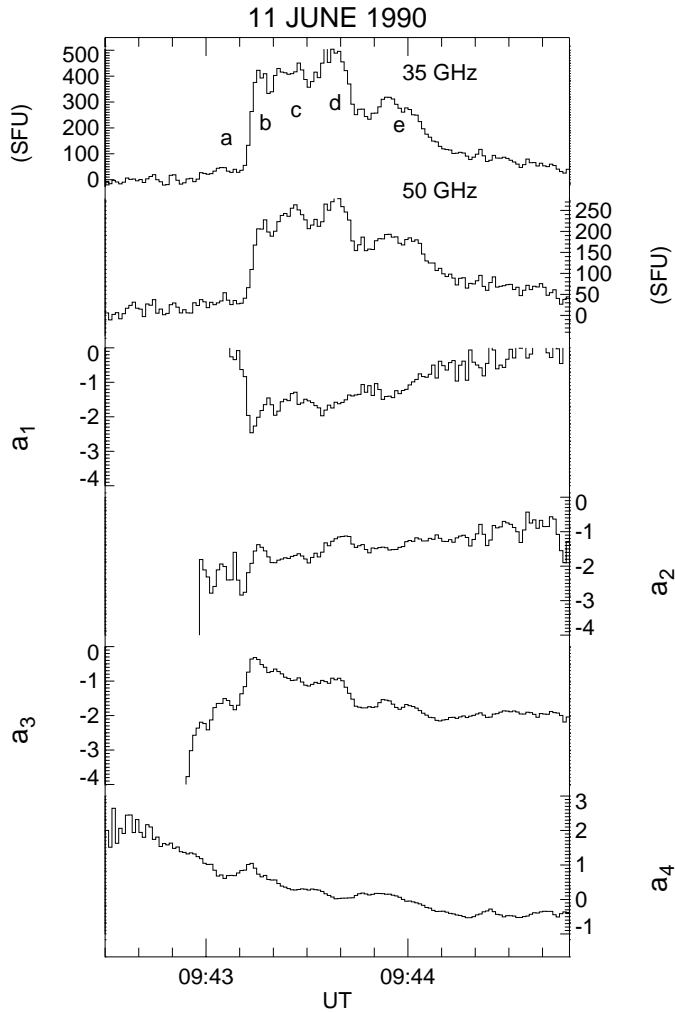


Fig. 4. Time evolution of the 35 and 50 GHz radio flux density (Bern polarimeters) and of the power law index of the centimetric-millimetric spectrum in different frequency intervals (see text)

3.2. Centimetric and millimetric radio observations

Centimetric-millimetric emission is observed during the whole HXR/GR burst in the available 3–50 GHz range of observing frequencies. Fig. 3 shows the time evolution of the radio flux density at 5.2 GHz (optically thick part of the spectrum), 35 GHz (optically thin part of the spectrum) and 11.8 GHz (around the turnover frequency f_{\max}). For comparison the 0.12–0.15 MeV and 0.32–0.57 MeV HXR count rates are also displayed. The time profile of the optically thin centimetric-millimetric emission is similar to that of the 0.12–0.15 MeV HXR emission. While peaks b, c, d and e are clearly seen at both 35 and 50 GHz, peak a is detected up to 35 GHz and barely visible at 50 GHz (see Fig. 4). Peak f is also seen in the optically thin part of the centimetric-millimetric spectrum up to 19.6 GHz.

From the start of the centimetric-millimetric event until ~ 0944 UT, the turnover frequency f_{\max} lies between 11.8 GHz and 19.6 GHz. At ~ 0944 UT, f_{\max} starts to drift towards lower frequencies. After $\sim 0944:13$ UT f_{\max} is less than 5.2 GHz. Between two successive observing frequencies the shape of the

centimetric-millimetric spectrum has been taken as a power law of the form f^a . Fig. 4 displays the time profiles at 35 GHz and 50 GHz together with the temporal evolution of the spectral indices a_1 , a_2 , a_3 and a_4 determined respectively between 50 and 35 GHz, 35 and 19.6 GHz, 19.6 and 11.8 GHz and 8.4 and 5.2 GHz. Fig. 4 shows that these spectral indices are time variable. For the optically thin part of the spectrum: (i) $a_2 \approx -1.5$ during peak a; (ii) a_1 remains relatively constant around -1.5 during peaks b, c, d and e; (iii) during the decay phase of the centimetric-millimetric event (after $\sim 0943:53$ UT) a_1 and a_2 increase from ≈ -1.5 to ≈ -0.5 , while a_3 remains around -2 and a_4 becomes negative after 0944 UT.

3.3. Metric and decimetric radio observations

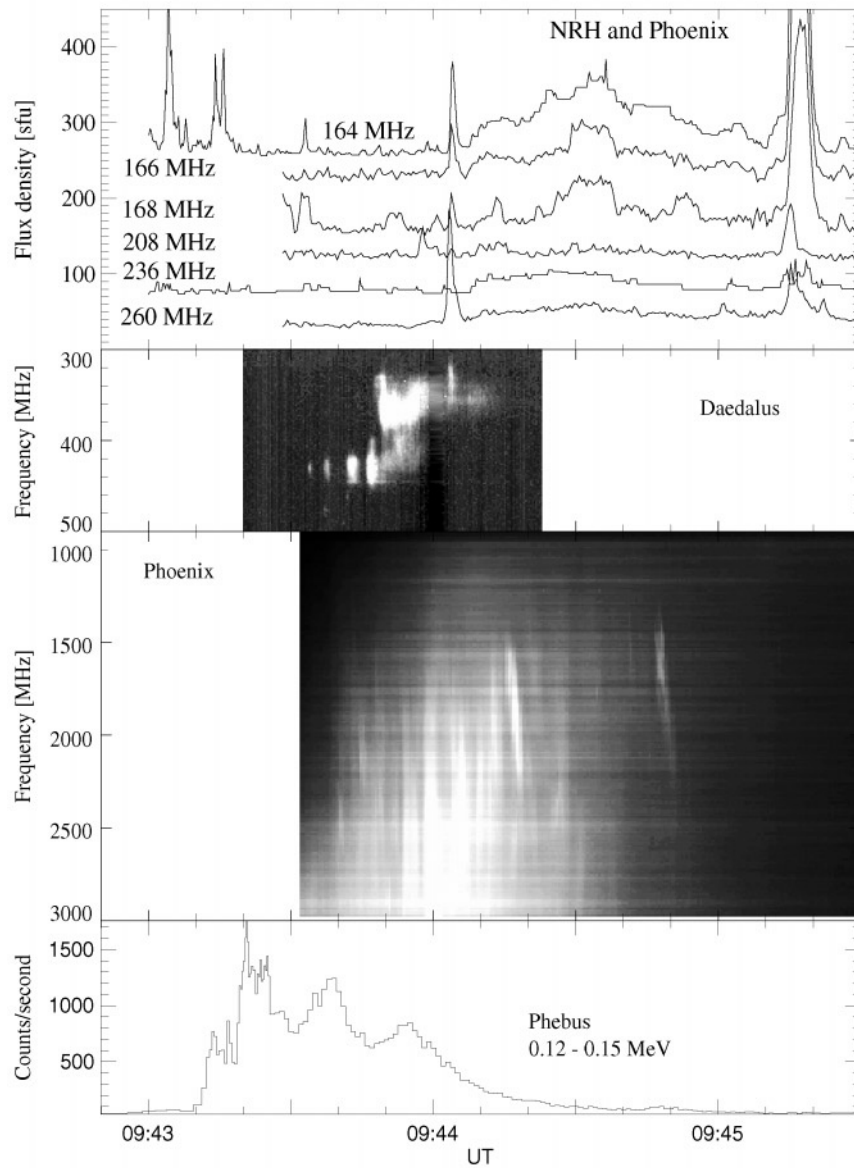
In Fig. 5, the 0.12–0.15 MeV HXR count rate is compared with metric and decimetric radio emission. The Phoenix spectrometer was programmed to trigger data recording for enhanced flux below 2 GHz. It started recording at 0943:32 UT (see the spectrogram from 0.9 to 3.0 GHz in Fig. 5). Also shown in Fig. 5 is the radio dynamic spectrum recorded in the ≈ 300 –500 MHz range by Daedalus and the time profile of the radio flux density recorded at six metric frequencies by PHOENIX and the NRH. The positions of the radio emitting sources observed with the NRH at 164 MHz, 236.6 MHz, 327 MHz, 408 MHz and 435 MHz are shown in Fig. 6 during four intervals of time. The locations of active regions NOAA 6089 (where the H α flare occurred) and NOAA 6095 are also indicated. The main characteristics of the radio emission in the metric-decimetric range and the comparison between HXR and radio observations during the four time intervals marked in Fig. 6 are outlined below (see also Table 3 for a summary).

0943–0943:33 UT (peaks a, b, c) From the onset of the 0.12–0.15 MeV emission to the onset of the 10–56 MeV emission (peaks a, b, c) the only emission observed by the NRH and DAEDALUS instruments in the 100–1000 MHz domain is a weak pre-existing noise storm. Its intensity is not significantly modified during the flare. The bursts seen on the 164 MHz time profile (Fig. 5) are type I bursts associated with the noise storm activity. Since PHOENIX observations were not triggered during this time interval, no significant radio emission was present in the 1–2 GHz domain.

0943:33–0943:45 UT (peak d) This time interval starts with the onset of the 10–56 MeV HXR/GR emission (peak d) which remarkably coincides with the onset of the decimetric radio emission. Radio emission is only observed at frequencies higher than 375 MHz. A detailed inspection of the time profile of the radio flux at different frequencies shows that in the 375–550 MHz band the emission consists of a succession of discrete type III bursts which are weakly polarized ($< 5\%$ right handed). The lack of both continuum and type III emission below 375 MHz indicates that electrons remain confined in magnetic loops which do not reach the high corona. This cutoff frequency (375 MHz)

Table 3. Synopsis of radio emissions during the different HXR/GR peaks.

Time interval (UT)	0943-0943:33	0943:33-0943:45	0943:45-0944:03	after 0944:03
HXR/GR	peaks a,b,c	peak d up to 56 MeV	peak e	decay and peak f
decimetric-metric	no flare related emission	III _{dm} 550-375 MHz	III _{dm} , RS 450-300 MHz	continuum <260 MHz
1-3 GHz (PHOENIX)	no trigger till 0943:32 UT	IV _{dm} , P, III _{dm} , RS	IV _{dm} , P, III _{dm} , RS	IV P, III _{dm} , RS
3-50 GHz (Bern)	$11.8 \leq f_{\max} \leq 19.6$ GHz	$11.8 \leq f_{\max} \leq 19.6$ GHz	$11.8 \leq f_{\max} \leq 19.6$ GHz	f_{\max} decreases $f_{\max} < 5.2$ GHz after 0944:13 UT

**Fig. 5.** The top panel shows the time evolution of the radio flux density observed at 260, 236, 208, 168, 166 and 164 MHz by the NRH and PHOENIX instruments (an offset of -20 , 30 , 104 , 110 , 170 and 230 sfu has been respectively added to the actual flux density). The two middle panels display the radio dynamic spectra recorded by DAEDALUS and PHOENIX in the 300-500 MHz and 1000-3000 MHz bands respectively. For comparison the time history of the 0.12-0.15 MeV count rate measured by PHEBUS is plotted in the bottom panel

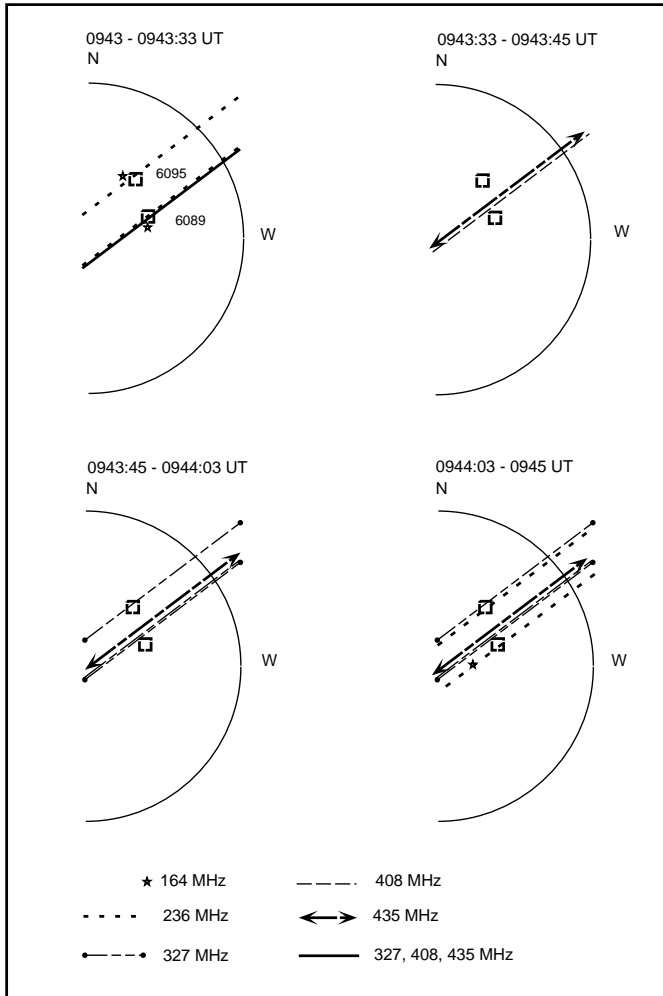


Fig. 6. Location of the 164, 236, 327, 408 and 435 MHz radio emitting sources obtained with the NRH during the four time intervals discussed in Sect. 3.3. The squares give the locations of NOAA regions 6089 (where the flare occurred) and 6095

must correspond to the plasma frequency (or its harmonic) of the top of the loops, indicating an electron density of $1.8 \cdot 10^9 \text{ cm}^{-3}$ (resp. $4.5 \cdot 10^8 \text{ cm}^{-3}$). Fig. 6 shows that the 408 MHz and 435 MHz emitting sources are on a line located to the north of the flaring region.

The beginning of this time interval (0943:33UT) is also associated with the onset of a decimetric type IV burst observed from about 0.6 GHz to beyond 3 GHz (Fig. 5). This emission is produced by a different mechanism than the centimetric-millimetric continuum discussed in the preceding section. It is generally believed to be caused by non-thermal electrons trapped in loops radiating at the upper-hybrid frequency $f_{\text{uh}} = (f_p^2 + f_e^2)^{\frac{1}{2}}$ (where f_p and f_e are respectively the electron plasma frequency and gyrofrequency). The low frequency cutoff (~ 0.6 GHz) suggests that these loops are denser than the loops outlined by the metric-decimetric emission (since usually $f_e \ll f_p$ in the solar corona). The circular polarization of the type IV burst is opposite to the one of the type III bursts.

0943:45-0944:03 UT (peak e) This time interval starts at the end of the significant emission above ~ 4 MeV, which approximately coincides with the beginning of peak e. Its end corresponds to that of the HXR/GR emission above 0.32 MeV. Fig. 5 shows that from $\sim 0943:45$ UT, the metric-decimetric radio emission, which was previously detected only above 375 MHz, suddenly extends towards lower frequencies (down to ~ 300 MHz). The radio spectrum consists of type III and of a continuum emission, usually referred to as type V radiation. The low frequency cutoff (~ 300 MHz) of the continuum suggests that, here again, electrons are confined in loops. However these loops are roughly half as dense (thus probably of larger scale) than those involved during the previous interval of time. The brightest features, observed between 300 MHz and 350 MHz, are not polarized. Fig. 6 shows that while the 408 MHz and 435 MHz emitting sources remain on the same line as during the previous time interval, the 327 MHz radio bursts arise from two spatially distinct sources. The intensity ratio of the two 327 MHz sources is about 1 to 8. Both sources have a similar time evolution of their flux density with coincident peaks (within ± 0.25 s). This indicates that the two sources are signatures of a common electron injection into two different loops or loop systems.

At frequencies above 1 GHz, PHOENIX has identified some decimetric type III and reverse drift bursts among the pulsations of the type IV continuum. They differ from the continuum by their opposite sense of polarization (left-hand circular).

0944:03-0945 UT (decay phase and peak f) This time interval covers the decay phases of the 300-450 MHz radio event and of the 0.12-0.32 MeV HXR/GR emission. A detailed inspection of Figs. 1 and 5 shows that the HXR decay is not smooth, but exhibits blurred time-structures. The first of these time structures roughly coincides with a type III burst at 0944:03 UT and with the onset of a faint continuum emission observed below 260 MHz. This low frequency continuum does not correspond to an enhancement of the preexisting noise storm at low frequencies because: (i) contrary to the noise storm emission, the continuum emission is unpolarized; (ii) at 164 MHz the source of the continuum lies at a significantly different position from that of the southernmost 164 MHz noise storm source (see Fig. 6). At 236.6 MHz two sources are observed, their spatial distribution being similar to that observed at 327 MHz during the previous time interval. The continuum radiation below 260 MHz and the 0.12-0.15 MeV HXR/GR emission vanish together around 0944:55 UT. At $\sim 0945:15-20$ UT metric type III bursts are observed below 260 MHz with no counterpart at higher radio frequencies and in the HXR/GR domain.

At frequencies above 1 GHz, PHOENIX identifies several reverse drift bursts (see Fig. 5) superposed on the pulsations of the continuum as in the previous time interval. The bursts show however a decreasing minimum frequency compared to those of the previous interval (1.8 GHz at 0943:42 UT and 1.6 GHz at 0944:47 UT) indicating a decreasing density in the source.

In summary, we note that the coherent radio emissions produced by beamed or/and trapped electrons are all consistent with closed magnetic field lines. However, the burst characteristics change step-wise from one time interval to the other. The evolution is not arbitrary. It has a trend from initial structures too small for loss cone and/or beam instabilities to develop, to larger and larger loops where these processes can occur at frequencies above 1 GHz. A second, much larger loop system where the 0.1-1 GHz emissions originate becomes also accessible simultaneously with the changes in the small structures. This second large loop system has also increasing dimension as the flare progresses.

4. Discussion

4.1. Energy content in accelerated electrons and protons

Previous studies of the 1990 June 11 HXR/GR burst have shown that the ~ 100 keV HXR flux exhibits fast time variations on time-scales ranging from ~ 0.2 s to 0.5 s (Talon et al. 1993b; Vilmer et al. 1994a). The bulk of the HXR emission is thus most likely produced by thick target interaction of non thermal electrons in dense regions ($> 10^{12}$ cm $^{-3}$) where the collisional life time of 100 keV electrons is smaller than the duration of the fastest HXR pulses. This implies that the 100 keV HXR time profile mimics that of the electron production rate. Using, as a first approximation, the spectral parameters of the low energy part of the photon spectrum given in Table 1 for the total photon spectrum S and thick target calculations by Brown (1971) the total energy content in > 100 keV electrons, $W_e(> 100$ keV) is about $2.5 \cdot 10^{28}$ ergs. By extrapolating the observed spectrum down to 20 keV we get $W_e(> 20$ keV) $\sim 4 \cdot 10^{29}$ ergs. The energy content in flare accelerated electrons above 20 keV ranges from $\sim 10^{26}$ ergs for microflares (Lin et al. 1984) to $\sim 10^{34}$ ergs for giant flares (Kane et al. 1995) and lies in the range $\sim 10^{28}$ - 10^{32} ergs for most of the observed HXR flares (e.g. Crosby et al. 1993; Lu et al. 1993). The 1990 June 11 flare appears thus as a rather moderate HXR flare although a significant > 10 MeV GR emission is produced.

As stated in Sect. 3.1. the number of excess counts due to deexcitation lines, in the 4-7 MeV energy range, is less than 3σ above the continuum. This corresponds to an upper limit of ≈ 2 photons cm $^{-2}$ for the 4-7 MeV GRL fluence. For GRL events the power law index s_p of the interacting proton spectrum is found to range from about 3.5 to 4.5 (Ramaty et al. 1995). We take a typical value, $s_p=4$, and use yields of the 4-7 MeV deexcitation lines and of the 2.23 MeV line given in Ramaty et al. (1993) for ambient and interacting particle elemental compositions obtained for the 27 April 1981 event (Murphy et al. 1991). Assuming that the energy content in ions is twice the energy content in protons (see e.g. Miller et al. 1997), this leads to an upper limit of the total energy content in > 1 MeV ions of $W_i(> 1$ MeV) $< 3 \cdot 10^{29}$ ergs. Using $s_p = 3.5$ - 4.5 and the upper limit of the 4-7 MeV GRL fluence given above, we consistently find that the expected excess of counts due to the 2.23 MeV line falls below the 3σ level. From the analysis of 19 flares

detected by the Gamma-Ray Spectrometer on the Solar Maximum Mission, Ramaty et al. (1995) found that $W_i(> 1$ MeV) is comparable to $W_e(> 20$ keV). As already stated by Trottet & Vilmer (1997), the above estimates show that this may also be the case for the 1990 June 11 flare which has all the characteristics of electron-dominated events recognized by Rieger & Marschhäuser (1990).

4.2. Relationship between HXR/GR and centimetric-millimetric emitting electrons

The HXR/GR continuum is assumed to be produced by bremsstrahlung emission of flare accelerated electrons. It is well established that the same electrons also produce centimeter-wave and millimeterwave emission via gyrosynchrotron radiation. Numerous attempts have been made to relate quantitatively the bremsstrahlung and the gyrosynchrotron radiations. For impulsive flares, like the 1990 June 11 one, different results have been obtained. On the one hand it has been concluded that gyrosynchrotron emission is produced in high magnetic field regions (~ 1000 G) by rather low energy electrons (< 200 keV) (see e.g. Kai 1986; Nitta & Kosugi 1986; Kosugi et al. 1988). On the other hand it has been found that this emission is produced by high energy electrons (> 200 - 300 keV to > 1 MeV) in 300-400 G magnetic fields (see e.g. Gary 1985; Klein et al. 1985; Ramaty et al. 1994). Furthermore, millimeter wave emission has been attributed to high energy electrons around 1 MeV characterized by a very flat spectrum, much flatter than the one deduced from X-ray observations below 200 keV (White & Kundu, 1992; Kundu et al, 1994 and references therein). As suggested by Vilmer & Trottet (1997), one possible reason of such a discrepancy is the use, in most of the studies performed so far, of HXR/GR observations obtained in a limited energy range (most often below 500 keV) and of centimetric-millimetric observations made at only one or a few frequencies which does not allow to clearly determine the shape of the electron population nor the optical thickness of the medium. HXR/GR and centimetric-millimetric observations obtained during the 1990 June 11 event do not suffer from the above limitations. This provides a unique opportunity to investigate which part of the electron spectrum contributes most significantly to the optically thin centimetric-millimetric emission. A complete modelling taking into account the involved magnetic field geometry would be necessary to derive parameters like the electron numbers producing the HXR/GR and centimetric-millimetric emissions (see e.g. Klein et al. 1986; Pick et al. 1990). Metric-decimetric imaging and spectral observations discussed in Sect. 3.3. indicate that the involved magnetic structure is complex and evolving with time. Thus in the absence of HXR and/or centimetric-millimetric imaging observations, the present data set is insufficient to constrain such a sophisticated analysis.

In the following we only attempt to relate the spectral slopes of the bremsstrahlung and gyrosynchrotron emitting electrons. We consider three cases proposed in the literature, referred to below as: free propagation, turbulent trapping and perfect trapping. Let δ_X and δ_R be the spectral indices of the elec-

tron populations which produce respectively the HXR/GR and centimetric-millimetric radiations and γ be the spectral index of the HXR/GR photon spectrum. For the three cases considered here the relationship between δ_X and δ_R and γ can be obtained as follows:

- *Free propagation*: In this model accelerated electrons stream freely along the magnetic field and produce thick target HXR/GR emission in the chromosphere. The precipitating electron flux, F_X (electrons $\text{keV}^{-1} \text{s}^{-1}$), is known from the HXR/GR observations and $\delta_X^{thick} \approx \gamma + 1$ (e.g. Brown 1971). The centimetric-millimetric radio emission is related to the instantaneous number, N_R (electrons keV^{-1}), of electrons in the centimetric-millimetric source located above the HXR/GR source. $N_R \approx F_X \tau$, where τ is the time spent by the electrons in the centimetric-millimetric source. For free streaming electrons, $\tau \approx L/v_e$, where L is the centimetric-millimetric source extent and v_e the electron velocity along the magnetic field. Thus we get $\delta_R^{prec} \approx \delta_X^{thick} + 0.5 \approx \gamma + 1.5$ for electrons up to a few 100 keV and $\delta_R^{prec} \approx \delta_X^{thick} \approx \gamma + 1$ for higher energy electrons.
- *Turbulent trapping*: In this case electrons are partially trapped in the coronal portion of a magnetic loop where they produce the centimetric-millimetric emission. Electrons precipitating from the trap are responsible for the HXR/GR thick target emission. Such a model was considered in Ramaty et al. (1994) where τ is given by a turbulent diffusive trapping time which is independent of energy so that $\delta_R^{turb} \approx \delta_X^{thick} \approx \gamma + 1$.
- *Perfect trapping*: Here the centimetric-millimetric and HXR/GR emitting sources are assumed to be cospatial with the same electron population radiating both emissions. The HXR/GR emission is produced through thin target interactions (e.g. Brown 1971) so that we get $\delta_R^{trap} \approx \delta_X^{thin} \approx \gamma - 0.5$

For several of the HXR/GR peaks observed during the 1990 June 11 event, the photon spectrum exhibits a marked spectral hardening above a break energy E_b . No simple formulae are available in the literature to relate electron spectra to HXR/GR spectra when such a hardening is present. As a first approximation we use calculations performed for a single power law photon spectrum and apply them independently to each part (i.e. below and above E_b) of the observed photon spectra given in Table 2. This is equivalent to consider that the two slope photon spectrum is produced by two populations of electrons which interact in different regions. The values of electron spectral indices, δ_X are thus derived from the photon spectral indices, γ , under some simplifications. In particular:

- The thick target and the thin target calculations by Brown (1971) do not take into account the contribution of electron-electron bremsstrahlung, which may become significant above a few 100 keV. If this contribution is taken into account it leads to slightly steeper electron spectra (see e.g. computations for thick target interactions by Skibo (1993)

presented in Ramaty et al. (1993)). For example a photon index of 2 corresponds to an electron index of 3.2 instead of 3. Such a variation is small compared to the change of the electron index implied by that of the observed photon index (1.2 to 2) below and above E_b . The conclusions drawn below would thus still remain valid even if electron-electron bremsstrahlung was taken into account.

- It was assumed that the HXR/GR emission was produced by two independent populations of electrons with single power law spectra. An alternative hypothesis is that the HXR/GR emission is radiated by a single population of electrons the spectrum of which is harder at high energies. This again will not modify our conclusions. Indeed the spectral slopes will remain about the same although the effects of a spectral hardening in the electron spectrum will be seen at lower energies in X-rays because of the convolution of the electron spectrum by the bremsstrahlung cross sections.

Approximate calculations by Dulk & Marsh (1982) show that the expected slope, a , of the optically thin centimetric-millimetric spectrum is related to the spectral index of the electron population δ_R by: $a \approx 1.22 - 0.9\delta_R$. Thus we get $a^{prec} \approx 1.22 - 0.9(\gamma + 1.5)$ for free propagation at low energies, $a^{prec} = a^{turb} \approx 1.22 - 0.9(\gamma + 1)$ for free propagation at high energies and for turbulent trapping and $a^{trap} \approx 1.22 - 0.9(\gamma - 0.5)$ for perfect trapping. These estimations of a can only be applied to optically thin observing frequencies in the range 10-100 f_e (Dulk & Marsh 1982) and for electron spectra with no upper energy cutoff (Ramaty et al. 1994). This relationship is furthermore not greatly altered by the inhomogeneity in the emitting source (Klein & Trottet 1984). In this study, the slope of the centimetric-millimetric spectrum is derived from observations at 35 and 50 GHz or at 19 and 35 GHz. Thus the expected values of a are valid for magnetic fields in the range ~ 200 -1000 G, i.e. for typical magnetic field strengths quoted in the literature.

Table 4 gives the values of a^{prec} , a^{turb} and a^{trap} computed for each HXR/GR peak by using γ_1 and γ_2 , the slopes of the photon spectrum for $h\nu < E_b$ and $h\nu > E_b$ respectively (see Table 2). The measured slope of the centimetric-millimetric spectrum, given in Sect. 3.2., is $a_2 \approx -1.5$ during peak a and $a_1 \approx -1.5$ during peaks b, c, d and e. The comparison of these observed values with those quoted in Table 4 appeals the following comments:

- For most of the event (peaks c, d, e) the centimetric-millimetric emitting electrons must be related to those emitting the HXR/GR emission above E_b . The values of the centimetric-millimetric indices expected from the turbulent trapping or free propagation models agree reasonably well with the observed ones.
- The value of the observed centimetric-millimetric index during peak b seems to indicate that the high energy electron component of index ≈ 3 produced during peaks c, d, e is already present in the centimetric-millimetric source, even if it does not give rise to a detectable high energy HXR/GR emission.

Table 4. Spectral indices of the optically thin centimetric-millimetric spectrum expected from the HXR/GR photon spectrum measured during the different peaks (see text for the definition of the symbols)

HXR/GR peaks	a	b	c	d	e
$\gamma_1 (h\nu < E_b)$	4.0 ± 0.5	5.0 ± 0.1	4.4 ± 0.1	2.9 ± 0.1	4.2 ± 0.1
a^{prec}	-3.7	-4.6	-4.1	-2.7	-3.9
a^{turb}	-3.3	-4.2	-3.6	-2.3	-3.5
a^{trap}	-2.0	-2.8	-2.3	-0.9	-2.1
$\gamma_2 (h\nu > E_b)$			2.0 ± 0.1	1.7 ± 0.1	2.0 ± 0.1
a^{prec}			-1.5	-1.2	-1.5
a^{turb}			-1.5	-1.2	-1.5
a^{trap}			-0.1	+0.1	-0.1

- The only possibility that the centimetric-millimetric emission is related to the low energy HXR/GR component is during peak a, providing that the HXR/GR and centimetric-millimetric sources are identical (perfect trapping). This is unlikely because we have shown in Sect. 4.1. that the HXR/GR radiation is most likely produced in a thick target. As during peak b, this suggests that the harder electron component of index ≈ 3 is already at work.

In summary although the time profile of the optically thin centimetric-millimetric emission resembles more that of the low energy (~ 100 keV) than that of the $\gtrsim 300$ keV HXR/GR emission (see Fig. 3), the comparison of the centimetric-millimetric and HXR/GR spectral indices indicates that the centimetric-millimetric radiation is produced by the high energy part of the bremsstrahlung emitting electrons. Moreover our results strongly suggest that these high energy electrons have been accelerated since the very beginning of the flare, even if their flux is too small to produce a detectable HXR/GR emission. A similar suggestion was drawn from comparative studies of millimeter wave and HXR observations (Kundu et al. 1994 and references therein).

4.3. HXR/GR and centimetric-millimetric emissions during peak d

Table 2 shows that the spectral characteristics of the emission during peak d are quite different from those determined during the other peaks, in particular during peaks c and e. Indeed E_b is shifted from ~ 0.35 MeV to ~ 0.75 MeV, the HXR/GR spectrum below E_b is harder and there is significant > 10 MeV GR emission. The lack of significant deexcitation and 2.23 MeV line emission and the sharp rollover of the photon spectrum above ~ 56 MeV indicate that the HXR/GR emission is mostly electron bremsstrahlung. Although the flux of > 0.2 MeV HXR/GR emitting electrons substantially increases during peak d, such an increase of the electron flux is not reflected in the optically thin centimetric-millimetric emission. Indeed: (i) the turnover frequency and the slope of the centimetric-millimetric spectrum

remain the same as during peaks c and e (see Sect. 3.2.); (ii) the ratio of both the 35 GHz and 50 GHz flux densities to the 0.32-0.57 MeV HXR/GR count rate which stays about the same during peaks c and e decrease by a factor of ~ 3 during peak d. In the following we qualitatively discuss the implications of this apparent contradiction.

Bremsstrahlung radiation from relativistic electrons is strongly beamed along the particle velocity within a cone of width $\approx 1/\gamma_e$, where γ_e is the Lorentz factor. Thus high energy GR are produced by electrons moving toward the observer. For example, calculations by Dermer & Ramaty (1986) indicate that, for a monodirectional electron beam with spectral index 2.5 (i.e. an index consistent with the present observations at high energies), the > 10 MeV (resp. > 40 MeV) GR flux is reduced by ~ 10 (resp. ~ 100), if the angle between the line of sight and the beam velocity varies from 0° to 1° . This may, at least partly, explain the high energy rollover of the photon spectrum. Because the 1990 June 11 flare is located close to the disk center, it is reasonable to assume that the magnetic field is almost radial in the vicinity of the feet of the flaring loops. Thus the > 10 MeV GR emission is mostly radiated either by: (a) an almost isotropic electron population near the top of high density loops; (b) by electron beams propagating upward along the magnetic field.

In case (a) electrons are confined in high density, thus probably high magnetic field regions from which efficient gyrosynchrotron radiation is expected. As this is not observed at 35 GHz and 50 GHz, centimetric-millimetric emission may, for example, lack if the plasma frequency at the loop top is of the order of or larger than 50 GHz, i.e. if the density is $\gtrsim 10^{13}$ cm $^{-3}$ so that the < 50 GHz emission cannot escape. Such a scenario seems to be unlikely because efficient electron acceleration is not expected from such a high density medium.

Case b represents a plausible scenario, consistent with the ensemble of the present observations. The occurrence of type III bursts in large scale structures support the idea of electron beams moving upward along the magnetic field. These beams will not produce substantial centimetric-millimetric radiation from the loop legs because the observer views the magnetic

field under a small angle and because electrons, at least high energy ones, have to be strongly beamed towards the observer. Scattering by collision or waves may spread the electron angular distribution near the top of these large loops where the magnetic field is viewed at a large angle. The decimetric type IV could be a signature of such scattering waves. However the magnetic field strength is likely to be too low to produce a substantial increase of the 35 GHz and 50 GHz fluxes.

If the electron production region is located in the coronal part of flaring loops, upward moving electrons would result from reflection at mirror points located in the chromosphere (e.g. Vestrand et al. 1991). Model calculations indicate that the magnetic field and the density must increase with depth over comparable scale heights in order to get substantial high energy (> 10 MeV) GR emission from the reflected beam (e.g. MacKinnon & Brown 1989, 1990; McTiernan & Petrosian 1991). It should be finally remarked that the centimetric-millimetric emission observed during peak d is similar to that produced during peaks c and e so that the characteristics of the radiating electrons and the physical parameters of the emitting sources have not greatly changed. This strongly suggests that the electron population producing enhanced ~ 0.2 -56 MeV HXR/GR radiation and the magnetic structures in which these electrons propagate are different from those involved in the bulk production of the centimetric-millimetric emission. This is supported by the fact that the onset of the > 10 MeV emission nearly coincides with that of the metric-decimetric emission.

4.4. Magnetic structures and electron acceleration/transport

The spectrum as well as the spatial distribution of the metric-decimetric radio emission reveal step-wise changes with time (see Sect. 3.3.). These changes do not appear arbitrarily in time but coincide (within less than a few seconds) with the onsets of different HXR/GR peaks which, for thick target interactions (see Sect. 4.2.), directly reveal changes in the electron production rate. It is widely believed that electron acceleration takes place in low lying magnetic structures with typical scale lengths ranging from a few 10^3 to a few 10^4 km and typical densities in the range 10^9 - 10^{11} cm^{-3} (e.g. Benz & Kane 1986; Kane 1987; Benz & Aschwanden 1991; Klein 1994). Thus the small time delays between changes in the particle production rate and of the metric-decimetric emission patterns are short compared to typical propagation times of magnetohydrodynamic (MHD) waves from the acceleration site to the metric-decimetric emitting region (typical height of $\sim 10^5$ km or even more). We thus conclude that changes in the spatial distribution of radio sources reveal that during the successive episodes of acceleration, electrons are injected into different large-scale magnetic structures where they produce metric-decimetric emissions. Furthermore, it is unlikely that electrons have access to the different large-scale structures by diffusing across the magnetic field from a single acceleration site (as e.g. a single flaring loop) because such a mechanism is not efficient in a medium with density $> 10^9$ cm^{-3} and too slow to account for rapid changes (Achterberg & Kuijpers 1984). We thus suggest that the electron access to the

large-scale structure is a consequence of step-wise changes of the spatial distribution of the different flaring loops involved in the acceleration region. Correia et al (1995) have reported millimetric radio observations of one flare which support this scenario. Their observations show indeed that the spatial distribution of the 48 GHz emitting sources is complex and rapidly changing on time-scales of a few seconds to a few tens of seconds.

The results of the comparison of HXR/GR, and radio emissions observed during the 1990 June 11 event are consistent with earlier findings by de Jager & de Jonge (1978) that electron acceleration during flares results from a succession of acceleration episodes they referred to as “elementary flare burst (EFB)”. The present study provides some evidence that these EFB’s are successively emitted in different small scale (10^3 - 10^4 km) structures from which non-thermal electrons have access to different large scale ($\sim 10^5$ km) magnetic structures. From the onset of the 1990 June 11 flare to its decay phase large-scale structures of increasing size and decreasing density are involved (see Sect. 3.3.). Moreover it should be emphasized that during peaks a, b and c electrons are confined within rather low lying loops since there is no metric or decimetric emission. The acceleration of relativistic electrons giving rise to > 10 MeV GR, if any, is weak. However such an acceleration becomes dramatically more efficient, when suddenly the acceleration site is connected to larger-scale structures (peak d). Chupp et al. (1993) also reported that efficient acceleration of relativistic electrons and energetic protons occurs in coincidence with the sudden involvement of large-scale structures which were not activated at earlier times in the flare. This latter result and the present one may indicate that efficient production of high energy particles requires that the acceleration site is connected to large-scale coronal structures. This supports the suggestion by Kane et al. (1995) that during the most energetic flares (“giant flares”) a large fraction of the corona must contribute to the production of non-thermal particles.

5. Conclusion

The main results of this first multiwavelength analysis of an electron-dominated event, associated with an optical flare located close to the disk center, are the following ones:

1. Considering upper limits of the GRL excess fluence ($< 3\sigma$ above the bremsstrahlung continuum), the > 1 MeV/nuc. ion energy content ($\lesssim 3 \cdot 10^{29}$ ergs) is found to be comparable to the > 20 keV electron content ($\approx 4 \cdot 10^{29}$ ergs). Thus the near equipartition in energy between electrons and ions found for strong GRL flares (Ramaty et al. 1995) may also hold for the 1990 June 11 event, even if significant GRL emission was not detected. It should however be emphasized that the electron energy content of the present event is about one order of magnitude below the lowest value estimated for strong GRL flares (see Fig. 3 in Miller et al. 1997). The present analysis thus supports the suggestion by Cliver et al. (1994) that electron-dominated events may be considered as weak GRL flares.

2. The comparison of the spectral indices of the HXR/GR and optically thin centimetric-millimetric emissions indicates that this latter emission is radiated by electrons with energies in excess of 400-700 keV. It also provides strong evidence that these high energy electrons have been produced since the very beginning of the flare, even if their number is too small to generate a detectable > 400-700 keV HXR/GR signature.
3. Step-wise changes of the magnetic structures in which non-thermal electrons propagate during the different peaks of the HXR/GR emission are observed. Such a behaviour is not a peculiar characteristic of electron-dominated events. Similar results were indeed found for a few GRL flares (Chupp et al. 1993; Trottet et al. 1994). However, for the present flare, the evolution of the magnetic structures is not arbitrary. From the flare onset to its decay phase accelerated electrons have access to magnetic structures of increasing size and decreasing density. In particular, the main HXR/GR peak which corresponds to a strong increase of the $\gtrsim 200$ keV flux with GR emission up to ~ 56 MeV, coincides with the switch on of the metric-decimetric radio emission, i.e. when electrons have suddenly access to large-scale ($\sim 10^5$ km) magnetic structures. Similar analysis of other events are needed to investigate if this sudden evolution from compact to extended structures is a general characteristic of electron-dominated bursts.
4. As the optical flare is close to the disk center, the electron-dominated peak exhibiting GR emission up to ~ 56 MeV is most probably radiated by an upward moving population of electrons which is strongly beamed along the magnetic field. The data suggest that this beamed electron population is different from that radiating the bulk of the centimetric-millimetric emission during this peak. Metric-decimetric radio observations also suggest that the interplay between small and large scale magnetic structures may play a crucial role in producing the > 10 MeV GR emitting electrons. A deeper investigation of this problem, which is beyond the scope of this case study, would require the analysis of more events. In particular, the beaming of both the > 10 MeV GR emission and gyrosynchrotron radiation at high radio frequencies along the electron velocities and the strong dependency of the centimetric-millimetric flux on the viewing angle with respect to the magnetic field indicate that it would be crucial to compare observations for electron-dominated events associated with flares spread over all longitudes.

In conclusion, this case study of an electron-dominated event provides some evidence that these bursts may be globally considered as weak GRL flares as was pointed out by Cliver et al. (1994). It also strongly supports the suggestion by Rieger (1994) that hard electron-dominated transients are peculiar events superimposed on the bulk flare emission. In the present case the data suggest that the main electron-dominated peak is produced by electrons interacting in a magnetic structure which is different from those emitting the bulk of the HXR/GR and centimetric-millimetric emissions.

Acknowledgements. We are grateful to Dr. K.-L. Klein for his helpful comments and critical review of the manuscript. The research of the french co-authors has been supported by the Centre National d'Études Spatiales and by the Centre National de la Recherche Scientifique (Groupement de Recherche: "Magnétodynamique solaire et stellaire").

References

- Achterberg A., Kuijpers J., 1984, *A&A* 130,111
 Barat C., Cotin F., Niel M., et al., 1988, in *Nuclear Spectroscopy of Astrophysical Sources*, Share G.H., Gehrels N. (eds.), AIP Conf. Proc. 170, 395
 Benz A.O., Aschwanden M.J., 1991, in *Eruptive Solar Flares*, Svestka Z., Jackson B.V., Machado, M.E. (eds.), *Lecture Notes in Physics* 399, 361
 Benz A.O., Kane S.R., 1986, *Solar Phys.* 104, 179
 Benz A.O., Güdel M., Isliker H., Miskowicz S., Stehling W., 1991, *Solar Phys.* 133, 385
 Brown J.C., 1971, *Solar Phys.* 18, 489
 Chupp E.L., 1990, *Sci* 250, 229
 Chupp E.L., 1996, in *High Energy Solar Physics*, Ramaty R., Mandzhavidze N., Hua X.-M. (eds.), AIP Conf. Proc. 374, 3
 Chupp E.L., Trottet G., Marschhäuser H., et al., 1993, *A&A* 275, 602
 Cliver E.W., Crosby N.B., Dennis B.R., 1994, *ApJ* 426, 767
 Correia E., Costa J.E.R., Kaufmann P. et al., 1995, *Solar Phys.* 159, 143
 Croom, D.L. 1979, Jan. 1, *Solar Flare Millimeter Data*, Appleton Laboratory, Ditton Park, Slough, England
 Crosby N., Aschwanden M.J., Dennis B.R., 1993, *Solar Phys.* 143, 275
 Debrunner H., Lockwood J.A., Barat C., et al., 1997, *ApJ* 479, 997
 de Jager C., de Jonge G., 1978, *Solar Phys.* 58, 127
 Dermer C.D., Ramaty R., 1986, *ApJ* 301, 962
 Dulk G.A., Marsh K.A., 1982, *ApJ* 259, 350
 Forrest D.J., 1983, in *Positron-Electron Pairs in Astrophysics*, Burns M.L., Hardings A.K., Ramaty R. (eds.), AIP Conf. Proc. 447, 3
 Forrest D.J., Chupp E.L., 1983, *Nat* 305, 291
 Gary D.E., 1985, *ApJ* 297, 799
 Kai K., 1986, *Solar Phys.* 104, 235
 Kane S.R., 1987, *Solar Phys.* 113, 145
 Kane S.R., Hurley K., McTiernan J.M., et al., 1995, *ApJ* 446, L47
 Klein K.-L., 1994, in *Advances in Solar Physics*, Belvedere G., Rodonò M., Simnett G.M. (eds.), *Lecture Notes in Physics* 432, 261
 Klein K.-L., Trottet G., 1984, *A&A* 141, 67
 Klein K.-L., Pick M., Magun A., Dennis B.R., 1987, *Solar Phys.* 111, 225
 Klein K.-L., Trottet G., Magun A., 1986, *Solar Phys.* 104, 243
 Kosugi T., Dennis B.R., Kai K., 1988, *ApJ* 324, 1118
 Kundu M.R., White S.M., Gopalswamy N., Lim J., 1994, *ApJS* 90, 599
 Lin R.P., Schwartz R.A., Kane S.R., Pelling R.M., Hurley K., 1984, *ApJ* 283, 421
 Lu E.T., Hamilton R.J., McTiernan J.M., Bromund K.R., 1993, *ApJ* 412, 841
 MacKinnon A.L., Brown J.C., 1989, *A&A* 215, 371
 MacKinnon A.L., Brown J.C., 1990, *A&A* 232, 544
 Marschhäuser H., Rieger E., Kanbach G., 1993, in *High Energy Solar Phenomena - A new Era of Space Measurements*, Ryan J.M., Vestrand W.T. (eds.), AIP Conf. Proc. 294, 171
 McTiernan J.M., Petrosian V., 1991, *ApJ* 379, 381
 Miller J.A., Cargill P.J., Emslie G.A., et al., 1997, *JGR* 102, 14631
 Murphy R.J., Ramaty R., Kozlovsky B., Reames D.V., 1991, *ApJ* 371, 793

- Nitta N., Kosugi T., 1986, *Solar Phys.* 105, 73
- Pick M., Klein K.-L., Trottet G., 1990, *ApJS* 73, 165
- Ramaty R., Mandzhavidze N., Koslovsky B., Murphy R.J., 1995, *ApJ* 455, L193
- Ramaty R., Schwartz R.A., Enome S., Nakajima H., 1994, *ApJ* 436, 941
- Ramaty R., Mandzhavidze N., Koslovsky B., Skibo J.G., 1993, *Adv. Space Res.* 13, 284
- Raoult A., Pick M., Dennis B.R., Kane S.R., 1985, *ApJ* 299, 1027
- Rieger E., 1994, *ApJS* 90, 645
- Rieger E., Marschhäuser H., 1990, in *Max91/SMM Solar Flares: Max91 Workshop 3*, Winglee R.M., Kiplinger A.L. (eds.), p. 68
- Skibo J.G., 1993, Ph.D. thesis, University of Maryland
- Talon, R., Trottet, G., Vilmer, N., et al., 1993a, *Solar Phys.* 147, 137
- Talon, R., Barat, C., Dezalay, J.-P., et al., 1993b, *Adv. Space Res.* 13, 171
- Tarnstrom G.L., 1973, *Astron. Mitt. Eidg. Sternwarte Zürich*, No 317
- The Radioheliograph Group, 1983, *Solar Phys.* 88, 383
- The Radioheliograph Group, 1989, *Solar Phys.* 120, 193
- Trottet G., 1994, *Space Sci. Rev.* 68, 159
- Trottet G., Vilmer N., 1997, in *Solar and Heliospheric Plasma Physics*, Simnett G.M., Alissandrakis C.E., Vlahos L. (eds.), *Lecture notes in Physics* 489, 219
- Trottet G., Chupp E.L., Marschhäuser H., et al., 1994, *A&A* 288, 647
- Trottet G., Vilmer N., Barat C., et al., 1993a, *A&AS* 97, 337
- Trottet G., Vilmer N., Barat C., et al., 1993b, *Adv. Space Res.* 13, 285
- Vestrand W.T., 1991, *Phil. trans. R. Soc. London, Ser. A* 336, 349
- Vestrand W.T., 1988, *Solar Phys.* 118, 95
- Vestrand W.T., Forrest D.J., Rieger E., 1991, *Proc. 22d Int. Cosmic-Ray Conf. (Dublin)*, SH2.3-5, 69
- Vilmer N. Trottet G., 1997, in *Coronal Physics from Radio and Space Observations*, Trottet G. (ed.), *Lecture Notes in Physics* 483, 28
- Vilmer N., Trottet G., Barat C., et al., 1994a, *Space Sci. Rev.* 68, 233
- Vilmer N., Trottet G., Barat C., et al., 1994b, in *Advances in Solar Physics*, Belvedere G., Rodonò M., Simnett G.M. (eds.), *Lecture Notes in Physics* 432, 197
- White S.M., Kundu M.R., 1992, *Solar Phys.* 141, 347
- Wülser J.P., Canfield R.C., Rieger E., 1990, in *Proceedings of MAX 91 Workshop #3*, University of Colorado, Winglee R.M., Kiplinger A.L. (eds.), p.149